

Role of incoherent dynamics in determining the electrical response of exciton-polaron complexes in pulsed magnetic resonance

T. L. Keevers* and D. R. McCamey

School of Physics, UNSW, Sydney NSW 2052, Australia

(Received 24 April 2015; revised manuscript received 5 June 2015; published 24 June 2015)

Triplet-exciton polaron quenching can lead to large changes in sample conductivity in organic devices. The application of pulsed magnetic resonance leads to changes in the quenching process by coherently driving spin populations between different eigenstates. Here, we investigate the influence of the exciton-polaron dissociation, intersystem crossing, and recombination rates on the electrical response of a device following such resonant excitation. Although these incoherent processes often occur on time scales that are orders of magnitude slower than coherent mixing, we find that they have a major influence on the electrical response. For example, as the relative recombination and dissociation rates are varied, certain resonant transitions can become electrically invisible. We demonstrate that transitions between different regimes are determined by a dimensionless parameter $\chi = \frac{\tau_r}{\tau_d}$, the ratio of the recombination to the dissociation rate.

DOI: [10.1103/PhysRevB.91.245208](https://doi.org/10.1103/PhysRevB.91.245208)

PACS number(s): 76.30.-v

I. INTRODUCTION

Pulsed electrically detected magnetic resonance (pEDMR) provides a powerful platform for investigating the spin-selection rules that underlie the optical and electronic pathways in a range of amorphous materials [1]. It can effectively disentangle multiple energy and time scales [2], detect even single electrons [3], and it is intrinsically sensitive to the electronic pathways of interest [4]. Importantly, pEDMR can access coherent time-domain information, unlike quasistatic techniques such as magnetoconductance measurements.

In this paper, we investigate the relationship between coherent spin control and incoherent spin readout in a triplet-exciton polaron (TEP) mediated process. This process modifies the average charge-carrier mobility of lone polarons and is thought to be responsible for the large magnetic field effects seen in many organic devices [5]. Materials in which the effect is seen include poly[2-methoxy-5-(2-ethylhexyloxy)-1,4-phenylenevinylene] (MEH-PPV) [6], blends of poly[2-methoxy-5-(3,7-dimethyloctyloxy)-1,4-phenylenevinylene]:[6,6]-phenyl-C61-butyric acid methyl ester [7], and methyl-bridged ladder-type poly(*p*-phenylene) [8].

Unfortunately, little is known in relation to the time-domain dynamics of this process [6,9]. We develop a simple model for the transient response of an ensemble of exciton-polaron complexes that are able to dissociate or recombine. The change in conductivity is integrated to provide a net change in charge, and the strength of this observable can be reduced to a simple ratio between the two competing processes. We show that the visibility of particular spin-resonance transitions can be tuned by varying the dissociation and recombination rates, and in some circumstances transitions become electrically invisible. The transitions between the recombination-dominated, balanced, and dissociation-dominated regimes are captured by a dimensionless parameter $\chi = \frac{\tau_r}{\tau_d}$, the ratio of the recombination to dissociation rate. Thus incoherent dynamics are able to influence the electrical signal arising from coherent mixing,

even when their time scales may differ by several orders of magnitude.

pEDMR can conceptually be reduced to three essential steps [10]: The first is state preparation, in which the spin ensemble is brought into a well-defined steady state by applying constant voltage or optical excitation. This is followed by the application of short pulses of microwave radiation, which induce resonant spin mixing and modify the spin-level population distribution. Finally, the resonant driving is turned off and the spin ensemble is allowed to relax back to its steady state. During this period, the transient dynamics are monitored and subsequently used to reconstruct the spin dynamics that occurred during the mixing period [11].

This scheme is depicted graphically in Fig. 1. Ultimately, every triplet-exciton polaron complex must either (i) dissociate or (ii) recombine, as shown in Fig. 1(a). The overall probability of each of these outcomes will determine the spin-dependent current from the exciton-polaron complexes. By exciting one of the resonant transitions, shown in Figs. 1(b) and 1(c) (ii), we change the spin statistics and thus the overall reaction yield. After the resonant driving is turned off, the spin ensemble will dephase for a short period, followed by a long transient recovery shown in Fig. 1(d) (iv). This long recovery is used to perform spin readout and reconstruct the spin dynamics of the rapid driving period.

Theoretical and experimental studies of pEDMR have primarily focused on the coherent dynamics of the spin mixing step, which includes the transition frequencies [12], resonance positions [12], and the onset of spin beating [13,14]. This information has been synthesized to derive unique “Rabi fingerprints” for a coupled spin-1/2 pair. These fingerprints are used to characterize zero-field splitting [12,15,16] and electron-nuclear coupling [17]. Even studies investigating the incoherent aspects of spin evolution [18]—charge-carrier generation [19], relaxation [20], recombination [21], and dissociation [21]—usually do so in relation to their effects on the spin evolution during the mixing period. However, the incoherent dynamics will influence the overall device response through setting the initial spin polarization and determining the transient dynamics, and these will nontrivially impact the

*t.keevers@student.unsw.edu.au

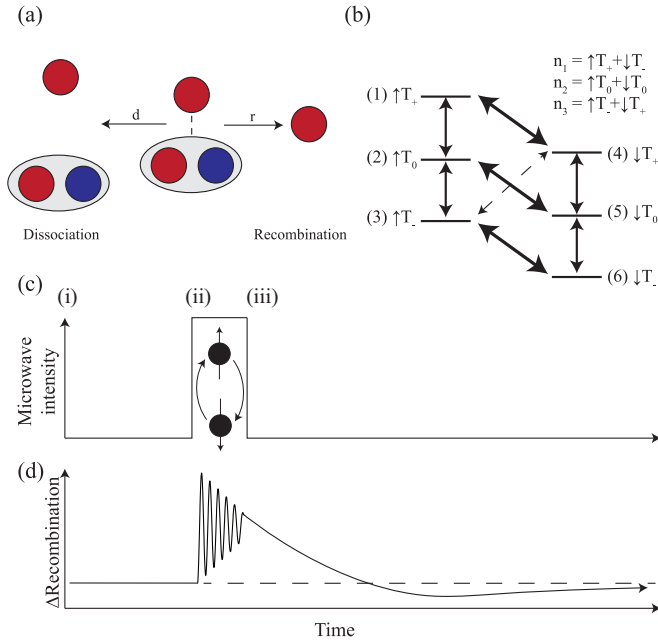


FIG. 1. (Color online) A conceptual sketch of pulsed electrically detected magnetic resonance. (a) A triplet-exciton and polaron can form a weakly spin-interacting, spatially bound complex that will either dissociate into a free exciton and trapped charge or recombine and detrapp the polaron. (b) The possible transitions of an exciton-polaron complex. There are three polaron transitions, four exciton transitions, and a nominally forbidden $|T_- \uparrow\rangle \leftrightarrow |T_+ \downarrow\rangle$ transition. (c) A conceptual schematic of pEDMR: (i) The spin ensemble is brought into a well-defined steady state. (ii) A microwave pulse is turned on, causing spin mixing between the doublet and quartet manifolds. (iii) A change in the quartet and doublet occupation leads to an overall change in the exciton-polaron recombination rate. This is seen as a transient change in current. (d) By integrating the transient, we are able to access the behavior of the spin ensemble during the short microwave pulse (image adapted from Boehme *et al.* [10]).

electrical response. This is true even when the spin-mixing period is entirely coherent.

Despite the rich information that can be accessed with pEDMR, a quantitative formalism for predicting the sign and magnitude of the electrical response is still elusive [22]. Modern theories of pEDMR are based on the Kaplan-Solomon-Mott (KSM) model [23], in which charge pairs form intermediate states spin-independently and can recombine spin-dependently. However, in some situations only one pair partner can be observed [24], and the relative contributions can be modified by the applied voltage [25] or illumination levels [26], temperature [1], or the static magnetic field [27] (B_0). A quantitative picture of the preparation and transient steps in pEDMR is a necessary ingredient for understanding these features.

The relationship between the incoherent spin dynamics and the observable was treated for continuous-wave electrically detected magnetic resonance by Lips *et al.* [28] and optically detected magnetic resonance by Movaghar *et al.* [29]. For these cases, the signal is intrinsically linked to the externally induced spin mixing and internal spin relaxation. In contrast, pulsed manipulation typically occurs within the coherence time with

a slower transient readout. The first transient pEDMR model was developed by Boehme and Lips [10], who modeled the competition between singlet recombination and Larmor beating. This was followed by Gliesche *et al.* [11], who extended the model by treating the observable as the integrated recombination response. One peculiarity of their scheme was that the observable was inseparable from the chosen integration limits. Finally, McCamey *et al.* [21] developed a more realistic transient model that included dissociation, and later intersystem crossing [18]. It was shown that the time constants and amplitudes of the transient quenching and enhancement could be used to estimate incoherent rates, and provide an upper bound for the intersystem crossing rate.

II. TRIPLET-EXCITON POLARON QUENCHING

Long-lived triplet excitons are able to diffuse through an organic polymer and form weakly coupled complexes with trapped polarons. These can dissociate back into a free exciton and a trapped polaron or, alternatively, recombine and detrapp the polaron causing a change in the sample conductivity [5]. Recombination is inherently spin-dependent and only occurs in the spin-1/2 (doublet) manifold, making it well suited for investigation with pEDMR. We have recently described the time-domain characteristics of this mechanism and shown that to first order, the exciton and polaron can be treated as individual spins [9,30]. In the high-field approximation, the Hamiltonian reduces to

$$H_0 = g_p \mu_B S_p^z B_0 + g_{ex} \mu_B S_{ex}^z B_0 - D_{ex} [3S_{ex}^z S_{ex}^z - S_{ex} (S_{ex} + 1)], \quad (1)$$

where g is the Landé g factor, μ_B is the Bohr magneton, B_0 is the external magnetic field, D_{ex} is the dipolar coupling of the exciton, and S_p and S_{ex} are the spin operators of the polaron and exciton. Resonant driving will add a small perturbation to the Hamiltonian,

$$H_1(t) = g_p \mu_B S_p^x B_1 \cos(\omega_0 t) + g_{ex} \mu_B S_{ex}^x B_1 \cos(\omega_0 t), \quad (2)$$

where ω_0 is the frequency of the applied radiation, B_1 is the magnitude of the perturbation, and t is the time. From the static Hamiltonian (H_0), the six eigenstates can be derived for the triplet-exciton subspace:

$$|\Phi\rangle = \begin{bmatrix} |\uparrow T_+\rangle \\ |\uparrow T_0\rangle \\ |\uparrow T_-\rangle \\ |\downarrow T_+\rangle \\ |\downarrow T_0\rangle \\ |\downarrow T_-\rangle \end{bmatrix}, \quad (3)$$

where $|\Phi\rangle$ is a matrix of the basis kets. These states can be paired in terms of their overall doublet content: $|\uparrow T_+\rangle$ and $|\downarrow T_-\rangle$ (n_1 states, no doublet content), $|\uparrow T_0\rangle$ and $|\downarrow T_0\rangle$ (n_2 states, $\frac{1}{3}$ doublet content), and $|\uparrow T_-\rangle$ and $|\downarrow T_+\rangle$ (n_3 states, $\frac{2}{3}$ doublet content), and we will use this notation throughout the paper due to symmetries of the possible resonant transitions. In this work, we assume the simplest case in which dissociation is spin-independent, $d_{d(\text{oublet})} = d_{q(\text{uartet})} = d$, and recombination can only occur within the doublet manifold, $r_d = r, r_q = 0$. Here doublet refers to the spin-1/2 manifold and quartet

TABLE I. The recombination and dissociation rates for each of the eigenstates of the exciton-polaron complexes.

State	Recombination	Dissociation
$n_1 \begin{cases} \uparrow T_+\rangle \\ \downarrow T_-\rangle \end{cases}$	0	d
$n_2 \begin{cases} \uparrow T_0\rangle \\ \downarrow T_0\rangle \end{cases}$	$r/3$	d
$n_3 \begin{cases} \uparrow T_-\rangle \\ \downarrow T_+\rangle \end{cases}$	$2r/3$	d

refers to the spin-3/2 manifold. The overall dissociation and recombination rates for each state are given in Table I.

Resonant microwave radiation can induce either a polaron transition with a Rabi frequency of γB_1 or an exciton transition with a Rabi frequency of $\sqrt{2}\gamma B_1$ [2]. The conductivity change from either of these transitions will depend on the overall change in doublet content, as well as the recombination and dissociation rates of the complexes.

Although we treat a weakly coupled exciton-polaron complex, our analysis will hold generally for any weakly coupled spin-1+spin-1/2 system, such as a strongly coupled bipolaron interacting with a counterion [8].

III. STEADY STATE

We can describe the state of a mixed spin ensemble by a density matrix, defined by

$$\rho = \sum_i w_i |\Phi_i\rangle \langle \Phi_i|, \quad (4)$$

where ρ is the density matrix, w_i is the population of each state ($\sum w_i = 1$), and $|\Phi_i\rangle$ are basis kets [Eq. (3)]. Diagonal entries of the density matrix (ρ_{ii}) identify the population of each state, and off-diagonal entries (ρ_{ij}) quantify the coherence between two states i and j [2]. Since spins are rapidly dephased during the preparation and transient readout portions of a pEDMR experiment, we neglect the off-diagonal components and focus our discussion on the spin populations ρ_{ii} .

The spin ensemble will establish a steady state when the pair generation rate is equal to the pair loss rate through the recombination and dissociation channels, so that

$$\rho_{ii}^{\text{eq}} = \frac{G}{6(r_i + d_i)}, \quad (5)$$

where ρ_{ii}^{eq} is the steady-state occupation of each eigenstate, G is the total exciton-polaron complex generation rate, r_i is the recombination rate for each eigenstate, and d_i is the dissociation rate for each eigenstate. The dissociation and recombination rate of each state is proportional to its doublet and quartet projection,

$$r_i = r_d |\langle \Phi_i | D \rangle|^2 \quad (6)$$

and

$$d_i = d_d |\langle \Phi_i | D \rangle|^2 + d_q |\langle \Phi_i | Q \rangle|^2 = d, \quad (7)$$

where D and Q are the doublet and quartet manifolds. When recombination is slow, there will be a linear buildup of polarization between the different states proportional to

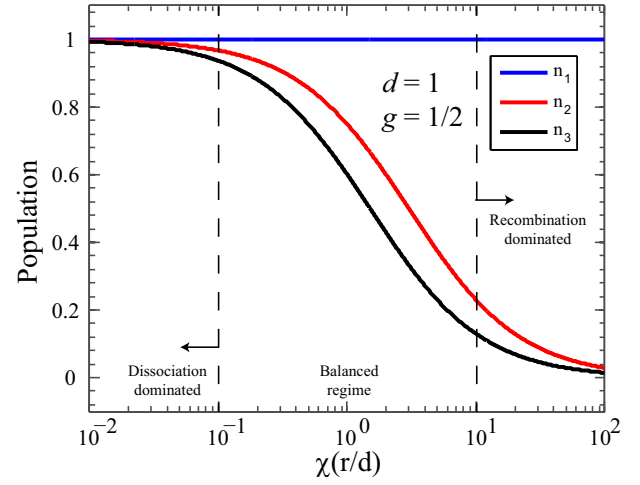


FIG. 2. (Color online) The steady-state occupation for each of the n_1 , n_2 , and n_3 states as a function of $\chi = \frac{r}{d}$ with a constant dissociation rate. The n_1 state occupation is independent of recombination, while the n_2 and n_3 state populations vanish asymptotically.

the relative recombination rate $\chi = \frac{r}{d}$. This results in a steady-state population given by

$$\rho_{ii}^{\text{eq}} = \frac{G}{6d} \begin{bmatrix} 1 \\ 1 - r/3d \\ 1 - 2r/3d \\ 1 - 2r/3d \\ 1 - r/3d \\ 1 \end{bmatrix}. \quad (8)$$

When the doublet recombination is extremely fast ($d \ll r$), only the pure-quartet states will be occupied and

$$\rho_{ii}^{\text{eq}} = \frac{G}{6d} \begin{bmatrix} 1 \\ 0 \\ 0 \\ 0 \\ 0 \\ 1 \end{bmatrix}. \quad (9)$$

The steady-state occupation will vary continuously between these two extremes, as shown in Fig. 2. The crossover between dissociation- and recombination-dominated behavior occurs around $r \approx d$. There is a large polarization buildup between the n_2 and n_3 states at the crossover point, and this has a direct effect on the visibility of the resonant transitions and is discussed throughout this paper.

IV. TRANSIENT DYNAMICS

The transient dynamics of the spin ensemble are described by the competition between a constant pair-generation rate and spin loss through recombination and dissociation. Due to Larmor beating between the exciton and polaron, phase coherence is quickly lost, and we can treat transient ensemble dynamics using rate equations [10]. The change in occupation of each state is quenched or enhanced following coherent spin mixing:

$$\dot{\rho}_{ii}(\tau) = \frac{G}{6} - (r_i + d_i)n_i(\tau), \quad (10)$$

where $\dot{\rho}_{ii}(\tau)$ is the rate of change in the spin population of each eigenstate, and n_i is the spin population of level i . Note that only the diagonal terms are nonzero. Integrating this gives

$$\rho_{ii}(\tau) = \rho_{ii}^{\text{eq}} + \Delta n_i(0)e^{-(r_i+d_i)\tau}, \quad (11)$$

where τ is the time after the resonant excitation and $\Delta n_i(0)$ is the change in spin population due to magnetic resonance. The transient current is proportional to the deviation of the instantaneous recombination rate from its steady-state value,

$$\Delta I(\tau) = e\Delta\mu \sum_i \Delta n_i(0)r_i e^{-(r_i+d_i)\tau}, \quad (12)$$

where ΔI is the (time-dependent) change in current following coherent driving, e is the charge of an electron, and $\Delta\mu$ is the average change in charge-carrier mobility of a released polaron as compared with a trapped one.

The transient will generally exhibit triexponential dynamics, however a biexponential will be seen when either (i) the quartet recombination rate vanishes ($r_Q = 0$) or (ii) the $n_1 \leftrightarrow n_3$ transition is excited and there is negligible intersystem crossing between the n_1 and n_3 states and the n_2 state. These scenarios can be differentiated by independently exciting the polaron ($n_1 \leftrightarrow n_3$) and exciton ($n_1 \leftrightarrow n_2$, $n_2 \leftrightarrow n_3$) transitions, and by performing additional experiments such as inversion recovery. Inversion recovery uses the pulse sequence $\pi - \tau_1 - \pi/2 - \tau_2 - \pi - \tau_2 - \pi/2 - \text{echo}$, where τ_1 is the inversion time and τ_2 is the refocusing time of the Hahn echo [2], to measure the incoherent spin-relaxation time T_1 .

Experiments on MEH-PPV organic light-emitting diodes (OLEDs) exhibit a biexponential decay [30] due to case (ii). If we assume that the slow time scale is d^{-1} and the faster time scale is $(d + \frac{2r}{3})^{-1}$, then we can fit a recombination rate of $r^{-1} = 47 \mu\text{s}$ and a dissociation rate of $d^{-1} = 559 \mu\text{s}$, which implies the exciton-polaron complex is in the strong recombination regime. The long lifetimes of the complexes are somewhat surprising considering the absence of a strong Coulombic attraction. This could be accounted for by the presence of the polarons in deep traps (reported as ~ 1 eV [31]), and a thermally activated dissociation process that is quenched at low temperatures.

V. OBSERVABLE

The transient changes in conductivity are conventionally converted to a change in charge through integration. This reduces the multidimensional dynamics to a single value, improves the signal-to-noise ratio, and provides a convenient measure of the spin-dependent conductivity. The general expression for the observable is

$$O = \int_{t_0}^{t_1} \Delta I(\tau) d\tau, \quad (13)$$

where O is the observable (net change in charge), and t_0 and t_1 are the transient integration limits. These are typically chosen by inspection to maximize the experimental signal-to-noise ratio. Throughout this text, we use the term ‘‘observable’’ to refer to the macroscopic changes in sample conductivity following spin manipulation. This is not to be confused

with the microscopic observable of singlet and triplet pair symmetry.

We can expand the expression for current to relate the change in charge [Eq. (12)] to the microscopic recombination and dissociation rates. Since we include non-negligible dissociation and assume fast Larmor beating, the observable reduces to

$$O = e\Delta\mu \sum_i \frac{r_i}{r_i + d_i} \Delta n_i e^{-(r_i+d_i)t_0} (1 - e^{-(r_i+d_i)(t_1-t_0)}). \quad (14)$$

If the integration period is extremely long ($t_0 \rightarrow 0, t_1 \rightarrow \infty$), then all recombination and dissociation events will be recorded, and we obtain

$$O = e\Delta\mu \sum_i \frac{r_i}{r_i + d_i} \Delta n_i. \quad (15)$$

This form is able to naturally and simultaneously account for both changes in conductivity and luminosity, and it eliminates the choice of arbitrary transient integration limits. The states are weighted by their probability of quenching, which characterizes the magnitude of magnetoresistance effects [32].

The electrical signal (O) will become distorted if t_0 or t_1 is poorly chosen. When the initial transient limit is too late [$(r_i + d_i)t_0 \gg 1$], the fast decaying components will be quenched, while an integration interval that is too short [$(r_i + d_i)(t_1 - t_0) \ll 1$] will filter out the slow decaying components. Inappropriate transient limits could arise from a long device or current amplifier RC constant (starting the transient too late) or using an inappropriately short shot repetition time (neglecting the slower components).

When the transient integration period becomes much shorter than the recombination and dissociation rates ($t_1 = 0, t_2 \ll r_i, d_i$), then the spin populations decay linearly [$e^{-(r_i+d_i)t_2} \rightarrow 1 - (r_i + d_i)t_2$] during the transient integration period, and the overall pair loss rate cancels out. Therefore, the observable becomes proportional to each states’ recombination rate,

$$O \approx t_1 e\Delta\mu \sum_i r_i \Delta n_i. \quad (16)$$

We conclude that the qualitative features of the observable are retained for a wide range of transient integration limits, except for ‘‘pathological’’ cases, thus justifying our treatment of a long transient integration period in this work. Mesoscopic device physics is necessary for a cogent description of magnetoresistance, and a complete description of the transient dynamics will probably require a similar treatment [33].

VI. TRANSITION VISIBILITY

We refer to the change in charge caused by a spin being transferred from level i to level j as the transition visibility (A_{ij}). It is related to the change in charge caused by a recombination event and the change in probability of recombination occurs after a spin is flipped. Thus a transition between two levels i and j has a visibility

$$A_{ij} = e\Delta\mu \left(\frac{r_j}{r_j + d_j} - \frac{r_i}{r_i + d_i} \right). \quad (17)$$

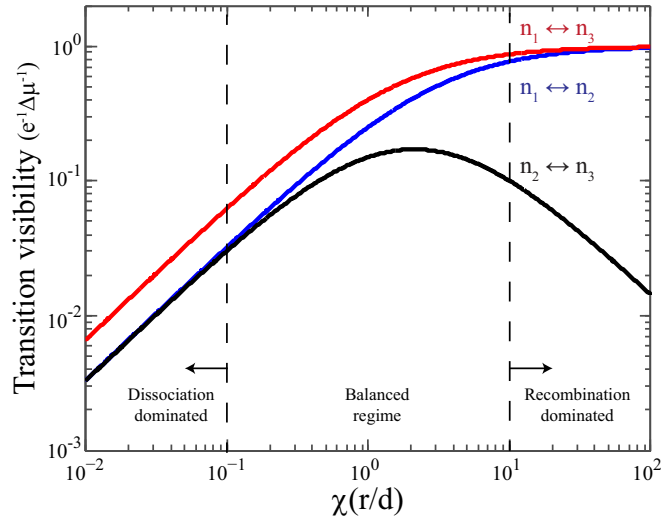


FIG. 3. (Color online) The transition visibility for an uncoupled exciton-polaron complex as a function of χ . In the slow recombination limit, the polaron transitions are twice as strong as the exciton transitions and there is a linear increase of all the transition visibilities with the recombination rate. As the recombination rate is increased further, the transitions between the quartet-doublet admixture states ($n_2 \leftrightarrow n_3$) become less visible as the probability of recombination for both states involved in the transition becomes unity. The transition visibilities for transitions involving the pure quartet state ($|\uparrow T_+\rangle$ and $|\downarrow T_-\rangle$) monotonically increase. The $|\uparrow T_0\rangle \leftrightarrow |\downarrow T_0\rangle$ and $|\uparrow T_-\rangle \leftrightarrow |\downarrow T_+\rangle$ transitions are not shown. These transitions are never visible, regardless of the recombination and dissociation rates.

The visibility of pEDMR differs significantly from those of cw- and pulsed-electron spin resonance (cwESR, pESR) experiments. In cwESR, the transition visibility is related to competition between off-diagonal coupling and spin relaxation,

$$S = \frac{\gamma B_1 T_2}{1 + (\Delta\omega T_2)^2 + (\gamma B_1)^2 T_1 T_2}, \quad (18)$$

where S is the signal strength, $\Delta\omega$ is the detuning, and T_1 and T_2 are the spin-relaxation times. Note that in cw-ESR, unlike in pEDMR, the signal will increase linearly with γB_1 for weak driving and vanish when driving is much faster than spin relaxation [$(\gamma B_1)^2 T_1 T_2 \rightarrow \infty$].

Meanwhile in pESR, the off-diagonal coupling represents the transition frequency

$$\Omega_R = |\langle \Phi_i | B_1 S_x | \Phi_j \rangle|, \quad (19)$$

where Ω_R is the Rabi frequency and the amplitude is determined by the net transfer of polarization [2].

The transition visibilities of pEDMR will strongly depend upon the relative recombination and dissociation rates, as shown in Fig. 3. When recombination is much slower than dissociation ($\chi < 0.1$, the “dissociation dominated” portion of Fig. 3), the $n_1 \leftrightarrow n_3$ polaron transitions will be twice as visible as the exciton transitions, and the visibility of each transition will scale linearly with the recombination rate.

In the opposite fast recombination limit ($\chi > 10$), only transitions involving the pure quartet states ($n_1 \leftrightarrow n_2$ and $n_1 \leftrightarrow n_3$) will be visible, and the recombination probability

will saturate. Transitions from the moderate (n_2) to high doublet content (n_3) states will cause no change in the integrated signal and will therefore be electrically invisible. This is shown in the “recombination dominated” portion of Fig. 3.

The $n_1 \leftrightarrow n_2$ and $n_1 \leftrightarrow n_3$ transitions become more visible as the recombination rate increases, while the visibility of the $n_2 \leftrightarrow n_3$ transition varies nonmonotonically with the recombination rate. $n_1 \leftrightarrow n_3$ transitions are most visible in the balanced regime ($0.1 < \chi < 10$), with a maximum when $r = \frac{3}{\sqrt{2}}d$, and transitions vanish in the limit of $r \rightarrow 0$ and $r \rightarrow \infty$, shown in Fig. 3. This counterintuitive behavior arises because of the conflicting requirements of large spin populations (slow recombination) and significantly different spin lifetimes (fast recombination).

VII. ELECTRICAL RESPONSE

The electrical signal (O) will depend on the total change in recombination, which is the product of the transferred polarization [which depends on the pulse sequence and the initial spin population, given by Eq. (8)] and the transition visibility [the signal per transferred spin, given in Eq. (17)]. An ideal pulse will completely transfer the two spin populations, so we can replace the transferred polarization with the initial population difference,

$$S_{ij} = \Delta n A_{ij} = (n_i - n_j) A_{ij}, \quad (20)$$

where S_{ij} is the total spin transfer from state i to state j , and n_i and n_j are the initial spin populations of levels i and j , which we assume are completely inverted. The population difference is related to the spin loss rates, while the visibility is related to the recombination probability. The electrical response can vanish or change sign when spin-dependent dissociation is also allowed: if the spin loss rate is identical for both populations ($r_i + d_i = r_j + d_j$), then there will be no net population transfer; similarly, if the probability of recombination remains constant ($\frac{r_i}{r_i + d_i} = \frac{r_j}{r_j + d_j}$), then no signal will be observed.

The electrical response for each transition is shown in Fig. 4 as the recombination rate is varied and the dissociation rate is kept constant. There is a monotonic increase in the electrical response of the $n_1 \leftrightarrow n_2$ and $n_1 \leftrightarrow n_3$ transitions with an increasing recombination rate due to both an increase in the spin polarization and an increase in the recombination probability in the n_2 and n_3 manifolds. In contrast, $n_2 \leftrightarrow n_3$ transitions will be invisible in both the weak and strong recombination regimes. When $r \approx 0$, neither state will have a significant probability of recombining, while $r \rightarrow \infty$ corresponds to both states being strongly depleted. The electrical responses peak at $d \approx r$, when there is the maximum difference in the n_2 and n_3 populations and recombination rates, however even under ideal circumstances the $n_2 \leftrightarrow n_3$ transitions do not produce large changes in current.

The overall electrical response is the product of the transition visibility and polarization. Substituting in the state occupation from Eq. (8) and the transition visibilities from Eq. (17) into Eq. (20), we can derive general expressions for the electrical response, given in Table II.

The transition amplitudes are sensitive to χ . When χ is small, all of the transitions will scale with χ^2 because the

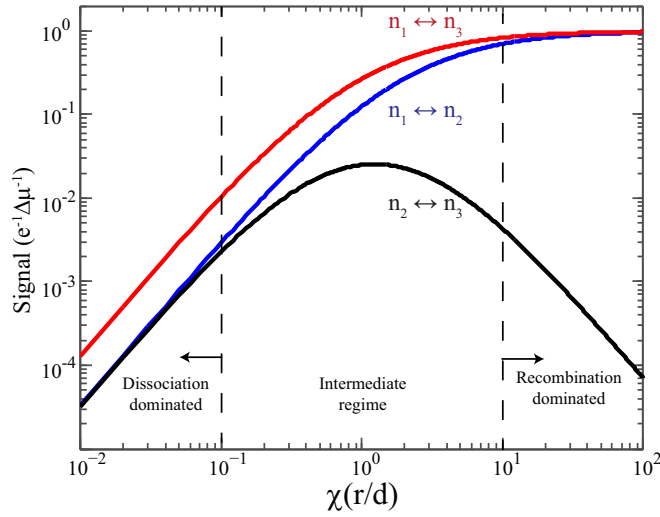


FIG. 4. (Color online) The normalized electrical response following a complete population inversion between two states as a function of χ with a constant dissociation rate, $d = \frac{G}{6}$. The steady state is calculated from Eq. (8) and the recombination probability is calculated from Eq. (17). The $n_1 \leftrightarrow n_2$ and $n_1 \leftrightarrow n_3$ transitions have a greater electrical response at high recombination rates, while the $n_2 \leftrightarrow n_3$ transition peaks at $r \approx d$. The signal is equal to the change in the probability of recombination following the indicated resonant transition. See the text for a complete description.

spin polarization and transition visibilities individually scale with χ . In the large recombination limit, the transitions from the pure quartet states will saturate with a response of $\frac{1}{d}$ (the number of complexes), and the electrical response to mixing the $n_2 \leftrightarrow n_3$ states will scale with $\frac{1}{\chi^2}$. This shows that pEDMR is most sensitive in systems in which competing spin-dependent processes have similar rates.

VIII. RESONANCE SPECTRUM

The resonance spectrum is used to estimate the zero-field splitting and Overhauser field distribution for spin pairs [21]: The external magnetic field is slowly stepped through, and at each position a nominal π -pulse is performed using weak

TABLE II. The normalized electrical response of possible exciton-polaron transitions in the slow and fast recombination limits where $\chi = \frac{r}{d}$ and G is the overall generation rate.

Transition	Signal, $S_{ij}/e\Delta\mu$	$\chi \rightarrow 0$	$\chi \rightarrow \infty$
(1)–(2)	$\frac{G}{6d} \left(\frac{\chi}{3+\chi}\right)^2$	$\frac{G\chi^2}{54d}$	$\frac{G}{6d}$
(1)–(4)	$\frac{G}{6d} \left(\frac{2\chi}{3+2\chi}\right)^2$	$\frac{2G\chi^2}{27d}$	$\frac{G}{6d}$
(2)–(3)	$\frac{G}{6d} \left(\frac{3\chi}{(3+\chi)(3+2\chi)}\right)^2$	$\frac{G\chi^2}{54d}$	$\frac{3G}{8d\chi^2}$
(2)–(5)	0	0	0
(3)–(4)	0	0	0
(3)–(6)	$\frac{G}{6d} \left(\frac{2\chi}{3+2\chi}\right)^2$	$\frac{2G\chi^2}{27d}$	$\frac{G}{6d}$
(4)–(5)	$\frac{G}{6d} \left(\frac{3\chi}{(3+\chi)(3+2\chi)}\right)^2$	$\frac{G\chi^2}{54d}$	$\frac{3G}{8d\chi^2}$
(5)–(6)	$\frac{G}{6d} \left(\frac{\chi}{3+\chi}\right)^2$	$\frac{G\chi^2}{54d}$	$\frac{G}{6d}$

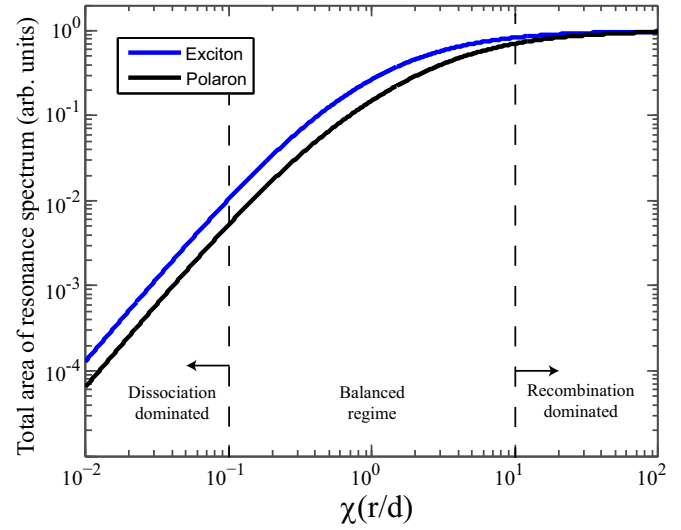


FIG. 5. (Color online) The normalized area of the polaron (black) and exciton (blue) components of the resonance spectra as a function of $\chi = \frac{r}{d}$ for a constant dissociation rate d . The polaron pattern has double the area of the exciton in the slow recombination limit. When recombination is fast, the two components will have equal area.

microwave radiation [21]. This last step ensures that spin beating and power broadening can be neglected. Although the theory of line-shape analysis is well developed for continuous-wave ESR, the foundations for pulsed methods are less established.

For the canonical case of weakly coupled polaron pairs, the resonance spectrum can be fit with two Gaussians [21]. A pulse length error will scale the overall resonance spectrum, but leave the relative amplitudes of the two components unchanged.

In contrast, the area of exciton and polaron components will depend on the initial polarization and transition visibilities. When recombination is slow, the polaron pattern will have twice the area of the exciton component, while in the fast recombination limit the integrated areas will be equal. The transition between these two regimes is shown in Fig. 5.

Another issue is that the polaron will have a resonance frequency of γB_1 , while the exciton will typically nutate at $\sqrt{2}\gamma B_1$. As such, the relative strength of the polaron and exciton contributions will vary as a function of pulse length, and either of the contributions may vanish for particular pulse durations. Great care must therefore be taken when extracting spectral information from pEDMR experiments.

Although ideally one would perform the full Rabi mapping experimentally, it is quite time-consuming to perform. The alternative, taking only a few slices, should work as long as reasonable pulse lengths are chosen. The visibility of the triplet exciton is primarily limited by its large dipolar splitting.

Finally, it is possible to use very long pulse lengths, so that the spin dynamics approaches the quasicontinuous-wave regime [16]. The powder pattern will resemble that of a continuous-wave experiment, which means the spectrum can be analyzed using more established theory. Unfortunately, this destroys phase information, which is one of the key benefits of pulsed experiments.

IX. SPIN BEATING

“Spin beating” or “spin locking” occurs when both spins in a pair nutate together under strong driving. For a weakly coupled spin-1/2 pair, such as polaron pairs or bipolarons, spin beating causes a suppression of the main γB_1 frequency and the simultaneous appearance of sum and difference components around 0 and $2\gamma B_1$ [13]. A similar effect can occur for an exciton-polaron complex when both species are simultaneously excited. When the number of spin pairs is conserved (short pulses), we can reduce the observable to

$$O = e\Delta\mu \sum_i \frac{r_i}{r_i + d_i} n_i. \quad (21)$$

This leads to

$$\begin{aligned} \frac{O(t)}{e\Delta\mu} = & \left(\frac{2\chi}{2\chi + 3} \right) [|\langle T_+ \downarrow | \Phi(t) \rangle|^2 + |\langle T_- \uparrow | \Phi(t) \rangle|^2] \\ & + \left(\frac{\chi}{\chi + 3} \right) [|\langle T_0 \uparrow | \Phi(t) \rangle|^2 + |\langle T_0 \downarrow | \Phi(t) \rangle|^2], \end{aligned} \quad (22)$$

where the eigenkets represent the occupation of each state.

The frequency components of a beating pair are readily calculated by substituting the time-dependent state occupation probabilities into the above equation, followed by a Fourier transform [13]. Without loss of generality, we perform this calculation for a pair initialized in the $|\uparrow T_+\rangle$ state. Beating pairs with other initial states will have identical spectra except for trivial changes in the signs of the frequency components. The frequency components and their amplitudes are plotted for an arbitrary recombination rate in Fig. 6 in terms of peak-to-peak changes in conductivity.

When a polaron pair starts to beat the main frequency, γB_1 will be suppressed, and its intensity will be split between the sum and difference components. In contrast, an exciton-polaron complex has fundamental frequencies of γB_1 and $\sqrt{2}\gamma B_1$, in addition to sum and difference beating components at $(\sqrt{2} \pm 1)\gamma B_1 \approx 0.4\gamma B_1$ and $2.4\gamma B_1$. Surprisingly, beating does not remove the fundamental γB_1 polaron component, but instead reduces its intensity by half and the $\sqrt{2}\gamma B_1$ exciton component can be completely quenched or only suppressed by a factor of $\frac{1}{2}$, depending on the recombination rate. The sum and difference components from spin beating will each have half the intensity of the polaron component. As in the polaron pair case, spin beating mainly redistributes the Fourier components and only modestly affects the overall intensity.

X. CONCLUSION

Triplet-exciton polaron complexes produce large conductivity changes in organic devices [5,8]. This process has been studied using static magnetoconductance spectroscopy [7], continuous-wave electron spin resonance [8], and pulsed electrically detected magnetic resonance [6]. The dynamic response of optoelectronic devices following pulsed magnetic resonance arises from a combination of coherent and incoherent dynamics. This is true even when the spin resonance occurs on the tens of nanosecond time scale—sometimes orders of magnitude faster than the incoherent dynamics. We

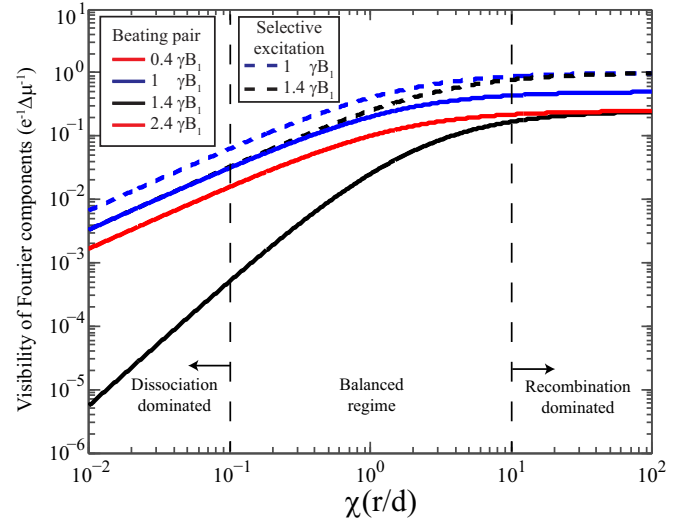


FIG. 6. (Color online) An exciton-polaron complex has Rabi frequencies of γB_1 (polaron), $\sqrt{2}\gamma B_1$ (exciton), and $\sqrt{2} \pm 1\gamma B_1$ (beating components). The strengths of the Fourier components are plotted as a function of χ . The dashed lines represent the individual polaron (blue) and exciton (black) resonances, and the solid lines represent the frequency spectrum for a beating pair. The signal is equal to the change in the probability of recombination following the indicated resonant transition. The red line represents both the sum and difference components, which have identical amplitudes. Simultaneous nutation causes the individual exciton and polaron frequencies to be diminished, and in the slow recombination limit the exciton component will vanish completely for a beating pair.

have studied the impact of the dissociation and recombination rates on the properties of exciton-polaron complexes, including their steady-state population, transition visibilities, resonance spectra, and spin beating components.

Our model predicts substantial qualitative changes as the recombination rate is tuned relative to the dissociation rate. The transitions between different regimes are determined by a dimensionless parameter $\chi = \frac{r}{d}$, the ratio of the recombination to dissociation rate. For example, certain exciton transitions can become electrically invisible when recombination is fast compared with dissociation ($\chi > 10$). In the dissociation-dominated regime ($\chi < 0.1$), polaron transitions produce a change in conductivity twice as large as those from exciton transitions. There will also be a fairly uniform steady state. Rapid recombination ($\chi > 10$) will produce a quartetlike steady state, close to $\frac{1}{2}(|\uparrow T_+\rangle\langle\uparrow T_+| + |\downarrow T_-\rangle\langle\downarrow T_-|)$. Certain transitions will produce no net change in the recombination rate and will be electrically invisible. Finally, in the balanced regime, there is a smooth transition between these two limiting cases.

ACKNOWLEDGMENTS

This work was supported by the Australian Research Council (ARC) (DP120102888). T.L.K. is supported by the Australian Renewable Energy Agency (ARENA)(7-S009). D.R.M. acknowledges an ARC Future Fellowship (FT130100214). We thank Joanna Guse for helpful discussions.

- [1] S. Baranovskii and O. Rubel, *Charge Transport in Disordered Materials* (Springer, West Sussex, 2007).
- [2] A. Schweiger and G. Jeschke, *Principles of Pulse Electron Paramagnetic Resonance* (Oxford University Press, Oxford, 2001).
- [3] M. Xiao, I. Martin, E. Yablonovitch, and H. Jiang, *Nature (London)* **430**, 435 (2004).
- [4] Z. V. Vardeny, *Organic Spintronics* (CRC, Boca Raton, FL, 2010).
- [5] P. Desai, P. Shakya, T. Kreouzis, W. P. Gillin, N. A. Morley, and M. R. J. Gibbs, *Phys. Rev. B* **75**, 094423 (2007).
- [6] W. J. Baker, D. R. McCamey, K. J. van Schooten, J. M. Lupton, and C. Boehme, *Phys. Rev. B* **84**, 165205 (2011).
- [7] P. Janssen, M. Cox, S. H. W. Wouters, M. Kemerink, M. M. Wienk, and B. Koopmans, *Nat. Commun.* **4**, 2286 (2013).
- [8] J. Shinar, *Laser Photon. Rev.* **6**, 767 (2012).
- [9] T. L. Keevers, W. J. Baker, and D. R. McCamey, *Phys. Rev. B* **91**, 205206 (2015).
- [10] C. Boehme and K. Lips, *Phys. Rev. B* **68**, 245105 (2003).
- [11] A. Gliesche, C. Michel, V. Rajevac, K. Lips, S. D. Baranovskii, F. Gebhard, and C. Boehme, *Phys. Rev. B* **77**, 245206 (2008).
- [12] M. E. Limes, J. Wang, W. J. Baker, S.-Y. Lee, B. Saam, and C. Boehme, *Phys. Rev. B* **87**, 165204 (2013).
- [13] R. Glenn, M. E. Limes, B. Saam, C. Boehme, and M. E. Raikh, *Phys. Rev. B* **87**, 165205 (2013).
- [14] S. Lee, S. Paik, D. McCamey, J. Yu, P. Burn, J. Lupton, and C. Boehme, *J. Am. Chem. Soc.* **133**, 2019 (2011).
- [15] J. M. Lupton, D. R. McCamey, and C. Boehme, *ChemPhysChem* **11**, 3040 (2010).
- [16] K. J. van Schooten, D. L. Baird, M. E. Limes, J. M. Lupton, and C. Boehme, *Nat. Commun.* **6**, 6688 (2015).
- [17] H. Malissa, M. Kavand, D. Waters, K. van Schooten, P. Burn, Z. Vardeny, B. Saam, J. Lupton, and C. Boehme, *Science* **345**, 1487 (2014).
- [18] D. R. McCamey, S.-Y. Lee, S.-Y. Paik, J. M. Lupton, and C. Boehme, *Phys. Rev. B* **82**, 125206 (2010).
- [19] J. Behrends, K. Lips, and C. Boehme, *Phys. Rev. B* **80**, 045207 (2009).
- [20] W. J. Baker, T. L. Keevers, J. M. Lupton, D. R. McCamey, and C. Boehme, *Phys. Rev. Lett.* **108**, 267601 (2012).
- [21] D. McCamey, H. Seipel, S. Paik, M. Walter, N. Borys, J. Lupton, and C. Boehme, *Nat. Mater.* **7**, 723 (2008).
- [22] J. Behrends, Ph.D. thesis, Freie Universität Berlin (2009).
- [23] D. Kaplan, I. Solomon, and N. Mott, *J. Phys. Lett. Paris* **39**, 51 (1978).
- [24] J.-M. Spaeth and H. Overhof, *Point Defects in Semiconductors and Insulators: Determination of Atomic and Electronic Structure from Paramagnetic Hyperfine Interactions* (Springer, Berlin, 2003), Vol. 51.
- [25] K. Lips, C. Boehme, and W. Fuhs, *IEE P-Circ. Dev. Syst.* **150**, 309 (2003).
- [26] S. Schaefer, S. Saremi, K. Fostiropoulos, J. Behrends, K. Lips, and W. Harneit, *Phys. Status Solidi B* **245**, 2120 (2008).
- [27] A. V. Barabanov, O. V. Tretiak, and V. A. Lvov, *Phys. Rev. B* **54**, 2571 (1996).
- [28] K. Lips, C. Lerner, and W. Fuhs, *J. Non-Cryst. Solids* **198**, 267 (1996).
- [29] B. Movaghar, B. Ries, and L. Schweitzer, *Philos. Mag. B* **41**, 159 (1980).
- [30] W. J. Baker, T. L. Keevers, C. Boehme, and D. R. McCamey, [arXiv:1502.05471](https://arxiv.org/abs/1502.05471) [*Phys. Rev. B* (to be published)].
- [31] H. Gomes, P. Stallinga, H. Rost, A. Holmes, M. Harrison, and R. Friend, *Appl. Phys. Lett.* **74**, 1144 (1999).
- [32] A. J. Schellekens, W. Wagemans, S. P. Kersten, P. A. Bobbert, and B. Koopmans, *Phys. Rev. B* **84**, 075204 (2011).
- [33] M. Cox, P. Janssen, F. Zhu, and B. Koopmans, *Phys. Rev. B* **88**, 035202 (2013).